Published online 25 February 2007 *Nucleic Acids Research, 2007, Vol. 35, No. 6* ***1761–1772***
doi:10.1093/nar/gkl1122

Pressure dissociation of integration host factor–DNA complexes reveals flexibility-dependent structural variation at the protein–DNA interface

Donald F. Senear[1,*], Vira Tretyachenko-Ladokhina[1], Michael L. Opel[2], Kimberly A. Aeling[2], G. Wesley Hatfield[2,3], Laurie M. Franklin[4], Reuben C. Darlington[4] and J.B. Alexander Ross[4]

[1]Department of Molecular Biology and Biochemistry, [2]Department of Microbiology and Molecular Genetics, College of Medicine, [3]Institute of Genomics and Bioinformatics, University of California, Irvine CA 92697 and [4]Department of Chemistry, The University of Montana, Missoula, MT 59812, USA

Received October 17, 2006; Revised December 9, 2006; Accepted December 10, 2006

ABSTRACT

E. coli **Integration host factor (IHF) condenses the bacterial nucleoid by wrapping DNA. Previously, we showed that DNA flexibility compensates for structural characteristics of the four consensus recognition elements associated with specific binding (Aeling *et al*., J. Biol. Chem. 281, 39236–39248, 2006). If elements are missing, high-affinity binding occurs only if DNA deformation energy is low. In contrast, if all elements are present, net binding energy is unaffected by deformation energy. We tested two hypotheses for this observation: in complexes containing all elements, (1) stiff DNA sequences are less bent upon binding IHF than flexible ones; or (2) DNA sequences with differing flexibility have interactions with IHF that compensate for unfavorable deformation energy. Time-resolved Förster resonance energy transfer (FRET) shows that global topologies are indistinguishable for three complexes with oligonucleotides of different flexibility. However, pressure perturbation shows that the volume change upon binding is smaller with increasing flexibility. We interpret these results in the context of Record and coworker's model for IHF binding (J. Mol. Biol. 310, 379–401, 2001). We propose that the volume changes reflect differences in hydration that arise from structural variation at IHF–DNA interfaces while the resulting energetic compensation maintains the same net binding energy.**

INTRODUCTION

Integration host factor (IHF) from *Escherichia coli*, is a 22 kD heterodimeric DNA-binding protein belonging to a general class of histone-like, DNA minor-groove-binding proteins that are present both in prokaryotes and eukaryotes (1,2). A characteristic feature of the DNA-bound complexes formed with IHF is extreme DNA deformation. A crystallographic model (3) of IHF bound to a 34 base-pair DNA fragment containing the H′ site of bacteriophage λ shows that the DNA is bent by more than 160° into a U-shaped conformation. In this model, DNA is wrapped across the top surface of the IHF dimer with one arm of the U lying along the side of each subunit, and close contacts are formed along the entire length of the DNA (Figure 1).

One function of IHF is to compact the 4.7 million base-pair circular bacterial DNA in the nucleoid, a complex assembly that includes other proteins and RNA (4). In this role, most cellular IHF binds DNA in a non-sequence-specific manner. However, unlike other proteins of its class, IHF also binds with much higher affinity to specific sites in the bacterial chromosome. DNA bending is also important because it helps to organize higher-level nucleo-protein structures that facilitate cellular functions, including lambda site-specific recombination (5), DNA replication (6) and gene transcription (7,8).

More than 170 specific IHF binding sites have been identified (9), and sequence consensus is limited to four small clusters of conserved bases located primarily in the 3′ half of the binding site (10–12). The two most highly conserved elements are the sequence, WATCAA, starting near the center of the site, and a second sequence, TTR, located four base pairs away in the 3′ direction (11).

*To whom correspondence should be addressed: Tel: (949) 824-8014; Fax: (949) 824-8551; Email: dfsenear@uci.edu
Correspondence may also be addressed to J.B. Alexander Ross. Tel: (406) 243-6026; Fax: (406) 243-4227; Email: sandy.ross@umontana.edu

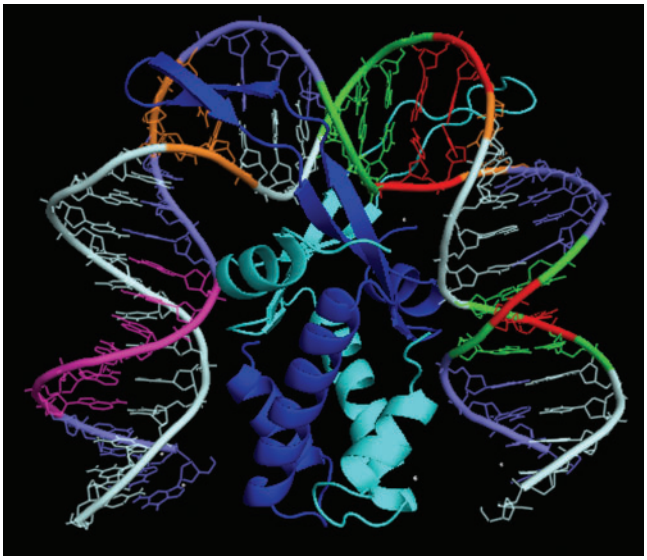

Figure 1. Crystallographic model of the complex of IHF bound to λ H′ site. The co-ordinate file for this structure, in which a nick in the sequence used to grow crystals (3) has been repaired, was supplied by Phoebe Rice (personal communication). The α and β subunits of IHF are shown in cyan and blue, respectively. Consensus DNA recognition elements are colored: (magenta) A-tract; (orange) ApA steps at proline intercalation sites; (red) direct interaction and (green) remaining base pairs of consensus, WATCAAnnnnTTR motif.

The DNA U-turn is centered near a third element consisting of two pairs of bases, most commonly AA, separated by nine base pairs in the middle of the binding site. Examination of crystal structures (3,13) shows that proline side chains at the tip of the β-ribbon arm of each IHF subunit are intercalated between these bases from the minor groove side of the DNA. This kinks the helix at these two locations to account for about half of the overall bend. Some IHF sites also contain a fourth element, a tract of four to six As in the 5′ half of the site (14,15). These four consensus elements constitute the essential features of the canonical IHF binding site. Sites that contain all of these elements are preferred over random sequences by ~2 500-fold (16–19). However, taken together, the consensus elements comprise only 15 to 17 of 34 base pairs, or less than half of the IHF binding site. The remaining 17 to 19 base pairs are not conserved.

The crystallographic models of several IHF–DNA complexes, featuring both wild type and a mutant IHF (3,13,20), have proven helpful towards developing an understanding of the mechanism of site specificity. In these structures, IHF contacts 26 backbone phosphate groups and also makes extensive interactions in the minor groove. Direct hydrogen bonds are made to three base pairs, but none involves a donor or acceptor that is unique to a particular base. Thus, recognition of the conserved elements can be explained completely in terms of sequence-dependent structural characteristics rather than as a consequence of direct readout interactions (5,21). The absence of base-pair-specific interactions in the major groove supports the widely held view that sequence recognition by IHF is entirely by indirect readout.

The observations that (1) site recognition is entirely by indirect readout and (2) the characteristic DNA bend involves, to a similar extent, both conserved and non-conserved sequences led us to consider how the unique features of the canonical sequence give sufficient favorable energy for specific binding of IHF while compensating for the large, unfavorable energy required to deform DNA (19). In particular, we asked whether the energy to deform a particular DNA sequence from its preferred B-form structure to the bent topology of the bound complex is a binding determinant. In other words, is DNA flexibility a component of the indirect readout mechanism? To answer this question, combinatorial sets of *de novo* DNA sequences were designed to systematically evaluate the influence of sequence-dependent structural characteristics of the conserved IHF recognition elements of the canonical IHF binding site, while the remaining sequence was varied to adjust the deformational energy required for the nearest-neighbor base pairs to adopt the characteristic DNA structure of the λ H′ DNA–IHF complex.

The results of the Aeling *et al.* (19) study on deformation energy indicated that DNA flexibility is able to substitute, to a substantial extent, for the structural characteristics of the conserved IHF recognition elements. 'That is, when one or more recognition elements are missing, the highest affinity binding is retained only in the limit of the lowest possible deformation energy. However, when all consensus sequence elements are present, the net binding energy is essentially unaffected by differences in deformation energies'. This point is illustrated by binding of IHF to a related group of sequences, referred to as Series A (19). These oligonucleotides each contain the recognition elements of the λ H′ sequence used in the original crystallographic analysis, but otherwise differ. The deformation energies of these sequences range from 82.9 to 141.9 kcal mol^{-1}. This variation is large in comparison to the net binding energies, which ranges only from −11.6 to −12.2 kcal mol^{-1} (Table 1).

In this report, we examine two hypotheses that could explain this surprising result. First, the topology of IHF complexes with Series A oligonucleotides may differ such that stiffer DNA sequences are bent to a lesser extent than sequences with greater flexibility, thus yielding similar binding affinity. This possibility is based on a thermodynamic model of IHF binding proposed by Record and coworkers (22,23). In this model, salt bridges between basic amino acid residues and DNA phosphates replace intra-molecular salt bridges within the protein. DNA bent to a lesser extent would require less deformation energy but at the energetic cost of formation of a smaller number of salt bridges with the protein.

Second, chemical interactions dictated by the different sequences comprising the canonical IHF–DNA complex could compensate in unique ways to yield similar net binding energies. For example, sequences with lower deformation energies will have different interactions than those with higher deformation energies. Interestingly, a consequence of the DNA–protein interactions proposed by Record and coworkers for IHF (22,23) is the absorption of water required to hydrate carboxylate side

Table 1. Binding and deformation energies for IHF binding to *de novo* synthetic sites

Site	Sequence	ΔG_{spec} (kcal mol^{-1})	Def. energy (kcal mol^{-1})
consensus	NNNAAAAAAN NNTTNCTWAT CAANNNNTTR NNNN		
A.2	ccgAAAAAAc tgTTactTAT CAAcgcgTTG cacc	−12.2	87
A.3	GccAAAAAAg caTTgctTAT CAAtttgTTG cacc	−11.7	92
A.6	cgtAAAAAAg atTTtctTAT CAAgtacTTG atgg	−11.6	142

Note: IHF binding to synthetic sequences designed to vary the deformation energy. Sequences contain the complete complement of consensus sequence elements as described in the text; the remaining sequence varies to generate the widest possible range of deformation energy. The consensus elements, shown in the first line for reference (W denotes A or T and R denotes purine), are colored to match the structural model shown in Figure 1. Values of the free energy change for specific binding (ΔG_{spec}) and the deformation energy when the sequence shown is threaded onto the repaired crystallographic structure of Rice (3,13) are from Aeling *et al.* (19).

chains in the complex and an unusually low salt dependence for complex formation. Given the expectation that water binding may have an important role in IHF association, subtle conformational changes affecting the amount of adsorbed water might be sufficient to balance the unfavorable deformation energy involved in achieving the U-conformation of the bent DNA in the canonical IHF complex.

To investigate these hypotheses, we first used time-resolved Förster resonance energy transfer (FRET) to evaluate the gross topologies of the IHF complexes with low- and high-deformation energy DNA sequences, as well as with the canonical DNA sequence. We then used high-hydrostatic pressure perturbation, with loss of steady-state FRET as the observable for dissociation, to explore the relationships between affinity of binding, salt-dependence of binding and volume change upon binding.

Time-resolved FRET supports the conclusion that the global topologies of the various complexes are the same. Hydrostatic pressure perturbation, however, reveals significant differences in the volume change for dissociation of the different high-affinity sequences. This indicates that the local topologies at the DNA–protein binding interface can differ significantly for different IHF-recognition sequences that have very similar specific binding affinity. Together, these observations suggest that the indistinguishable global topologies in the high-affinity sequences must result from base-pair deformations in different positions of these sequences as dictated by the position-specific variations in the canonical sequence. We propose that if DNA is deformed at the most flexible base-pair steps in these sequences, the impact of deformation energy is minimized. Furthermore, we propose that the observed variation in deformation energy is balanced by the formation of sequence-specific, favorable DNA–protein contacts that promote the appropriate high-affinity binding that is a characteristic of the canonical IHF site.

EXPERIMENTAL

Materials

Unless otherwise indicated, buffer components and reagents are reagent grade.

IHF purification and activity

IHF was purified according to Nash *et al.* (24). The specific DNA-binding activity of IHF was determined by conducting site-titrations to a high-affinity binding site ($K_d \sim 1 \times 10^{-9}$ M), as described by Aeling *et al.* (19). Aliquots were stored at -70°C and thawed immediately prior to use.

IHF-binding DNA oligonucleotides

The 50-base-pair DNA oligonucleotides used in the pressure-dissociation experiments were based on the sequence template

5′-GTTGGCAT—(X34)—GAACAGGT-3′

where X34 denotes a variable segment of sequence that corresponds either to different naturally occurring IHF binding sites or to sites designed to contain different combinations of IHF consensus recognition elements (12). The variations in X34 used in these experiments are listed in Table 1. As indicated in the template, the 5′ and 3′ eight-base-pair flanking sequences, which are from the λ H′ IHF binding site, were kept invariant. Gel-purified, dye-conjugated sense and anti-sense sequences of each site, labeled at the 5′ end via 6-carbon linkers to 6-FAM (6-carboxy fluorescein) and TAMRA (carboxy–tetramethyl rhodamine), respectively, were purchased from IDT (Coralville, IA). Double-strand oligonucleotides were generated by annealing 10 to 12 μM of each complementary single-strand oligonucleotide (1:1 ratio) in TE buffer (10 mM Tris, 1 mM EDTA and 0.1 M NaCl, pH 8) using a water bath at 85°C that was allowed to cool to room temperature overnight. Recovery and labeling efficiency were estimated from the UV/visible absorption spectrum, using extinction coefficients of 95 000 and 78 000 M^{-1} cm^{-1} at the absorption maxima for TAMRA and FAM (Molecular Probes, Inc.), respectively, and as calculated by IDT for the oligonucleotides. For example, on this basis, the efficiencies of labeling oligonucleotide A.2 with FAM and TAMRA were 94 and 85%, respectively.

Considerations for FRET

The efficiency of resonance energy transfer, E_T, is given by

$$E_T = \frac{R_o^6}{r^6 + R_o^6} = 1 - \frac{\tau_{DA}}{\tau_D} \quad (1)$$

where r is the distance of separation between donor and acceptor and R_o is the Förster distance at which the transfer efficiency is 50%; τ_{DA} is the donor lifetime in the presence of acceptor and τ_D is the donor lifetime in the absence of acceptor (25).

Like Lorenz and Diekmann (26–28), we used FAM and TAMRA as the donor–acceptor pair because this pair has a Förster distance of about 5 nm (29), and thus is ideally suited for studying changes in FRET distances of a few angstroms as might occur in different IHF–DNA complexes. In addition, if we assume that the free DNA is in B conformation, the donor and acceptor separation is about 16.5 nm for a 50-base-pair oligonucleotide. In this case, the probability of FRET for FAM/TAMRA is zero. Consequently, protein-free DNA does not contribute to FRET.

Fluorescence electrophoretic mobility shift assay

Mobility-shift titrations were conducted as site titrations. Reaction mixtures containing 100 nM double-labeled, double-stranded oligonucleotide A.2 (Table 1) and IHF at concentrations ranging from 0 to 240 nM in a 20-µl volume were prepared in binding buffer (10 mM Tris pH 8.0, 100 mM NaCl and 1 mM EDTA). After 10-min incubation at room temperature, the reaction mixtures were loaded at 25 V into the wells of BioRad, 10% acrylamide, TBE Readygel™ that had been pre-electrophoresed for 5 min at 200 V. Electrophoresis was continued for 40 min at 100 V. Wet gels were scanned at 100 µm resolution on a GE Healthcare Typhoon 9410 imager with 488 nm laser excitation and detection through a 520 nm/30 nm bandpass filter for FAM fluorescence and through a 580 nm/40 nm bandpass filter for TAMRA emission resulting from energy transfer. Gels were also scanned for direct TAMRA emission using 532 nm laser excitation.

Fluorescence lifetime measurements

Time-resolved fluorescence intensity decay data were collected using an ultra-fast, time-correlated, single-photon counting (TCSPC) instrument, described previously (30). Excitation was at 470 nm with 2 ps pulses (full-width at half-maximum) of vertically polarized laser light, at a repetition rate of 4.8 MHz. The emission optical path, at 90° to the excitation, passed through a polarizer oriented at 54.7° from vertical (the magic angle condition (25)) to eliminate intensity artifacts due to molecular rotation. The detection wavelength was selected by using a monochromator with a 20 nm band-pass. Intensity decay curves and corresponding instrument response functions (IRF) were collected with a timing calibration of 22 ps per channel into 2000 channels at counting rates of about 25 kHz or less to assure single-photon counting conditions. The decay curves were collected to 40 000 peak counts. The IRF for each decay curve was measured using a light-scattering solution of dilute colloidal silica and collected to 100 000 peak counts.

The intensity decay data sets were analyzed by a standard reconvolution procedure (31), using non-linear regression (32). The fluorescence intensity decay, $I(t)$, was fit to a sum of exponentials:

$$I(t) = \sum_{i=1}^{n} \alpha_i e^{-t/\tau_i} \quad (2)$$

where the pre-exponential factor α_i is the amplitude of each component and τ_i is the associated fluorescence lifetime.

Pressure-dissociation experiments using FRET as an observable

Pressure experiments were conducted using an SLM 4800 fluorometer modified in our laboratory for single-photon counting. The high-pressure sample chamber, similar in design to that described by Paladini and Weber (33), was constructed by the Physics Department machine shop at the University of Illinois, Urbana. The reaction mixtures contained IHF and FAM/TAMRA double-labeled oligonucleotides in the binding buffer described for the mobility-shift assays except as noted. Emission spectra from 490 to 650 nm were obtained at 20°C with excitation at 480 nm. Excitation and emission band-passes were 4 and 16 nm, respectively.

Dissociation of IHF from fluorophore-labeled DNA oligonucleotides was observed by the decrease in FRET with FAM as donor and TAMRA as acceptor. The extent of FRET was determined by comparing the change in the fluorescence emission intensities integrated between 515 and 525 nm, due to FAM, with those between 575 and 585 nm, primarily due to TAMRA. The latter wavelength interval minimizes the overlap between the low-energy tail of FAM emission and the high-energy onset of TAMRA emission. Following the approach described by Rietveld and Ferreira (34), the donor/acceptor emission intensity ratio was used to assess the FRET efficiency, with dissociation being characterized by the increase in the ratio.

As noted by Rietveld and Ferreira (34), there is a gradual decrease in the donor/acceptor emission ratio with increasing pressure in the absence of FRET. This is due to the pressure-dependent birefringence of the optical windows. Therefore, the change in the donor/acceptor emission ratio due to IHF dissociation was corrected using a baseline calculated from a polynomial fit to the pressure-dependent donor/acceptor emission ratio measured in the absence of IHF. Based on a two-state model in which DNA is either bound (high FRET) or free (low FRET), the apparent fraction of DNA bound was calculated as the fractional change in the baseline-corrected donor/acceptor emission intensity ratio.

Numerical analysis

Non-linear least squares analysis was conducted using Origin 7 software (OriginLab Corp.), which estimates parameter values corresponding to a minimum in the variance. Joint confidence limits, which account for correlation between parameters, are calculated by adjusting each parameter individually and refitting the others

while searching for a variance ratio as predicted by the *F*-statistic (35). Uncertainties in parameter values are reported at the 95% confidence level. When global analysis of multiple experiments was conducted, normalized weights were calculated for the individual data from the square roots of the variances of separate fits of the individual experiments.

RESULTS

Time-resolved FRET measurements were conducted to determine whether Series A IHF-binding oligonucleotides that have less flexible sequences are less bent than sequences with greater flexibility but similar IHF-binding affinity. High-hydrostatic pressure perturbation measurements were conducted to examine the relationships between deformation energy, salt-dependence of binding and volume change that together would favor similar 'net' binding energies for sequences with 'different' deformation energies. Oligonucleotides A.2 and A.6 were selected for these experiments because they are representative of sequences with low and high deformation energies, respectively. Oligonucleotide A.3 was also included because it contains the λ H′ site sequence, which has been the reference site for the majority of the structural (3,13) and thermodynamic investigations (22,23,40) of IHF–DNA binding.

Time-resolved FRET

The apparent distance between the two 5′ ends of the different oligonucleotides was determined from time-resolved FRET experiments by measuring the decrease in the fluorescence lifetime of FAM upon addition of IHF. A single lifetime of 3.95 ± 0.05 ns was obtained for FAM fluorescence of the different oligonucleotides. This value was unaffected by the presence of TAMRA, thus confirming no dynamic quenching of FAM fluorescence due to FRET or other processes when IHF is absent. In the presence of IHF, a second decay component with a shorter lifetime of 1.7 ± 0.1 ns was observed for the FAM fluorescence of the doubly labeled oligonucleotides. As would be expected for a site titration and a two-state equilibrium between bent and linear DNA, the amplitude of the 1.7 ns lifetime increased in proportion to IHF concentration until saturation was achieved, whereas the amplitude of the 3.95 ns lifetime decreased.

To confirm that the 1.7 ns lifetime was due to FRET, we repeated the gel electrophoresis IHF titration described by Lorenz and Diekmann (26), but with the reaction conditions used for time-resolved FRET measurements. As shown in Figure 2, addition of IHF to oligonucleotides end-labeled with FAM and TAMRA causes the appearance of a lower mobility band. With excitation of FAM at 488 nm, this band is marked by a reduction in FAM fluorescence and increase in TAMRA fluorescence, a spectroscopic signature of FRET. In contrast, the higher mobility band exhibits only green FAM fluorescence, indicating no FRET. Parallel to the amplitude changes of the 3.95 and 1.7 ns FAM lifetimes, increasing IHF concentration resulted in diminution of the intensity of the faster running, green fluorescent band and simultaneous increment in the intensity of the slower running, yellow fluorescent band. Direct excitation of TAMRA is inefficient at 488 nm and the yellow color results from a combination of green and red fluorescence from FAM and TAMRA, respectively, indicating efficient FRET due to the wrapped DNA in the bound complex.

Figure 2. Electrophoretic mobility-shift assay of IHF binding to oligonucleotide A.2. IHF concentrations in Lanes 1–10 are 0, 20, 40, 60, 81, 99, 120, 165, 201 and 240 nM, respectively. This pseudo-color image was generated by coloring the emission collected through a 520-nm band pass filter green (FAM fluorescence) and coloring the emission collected through a 580-nm band pass filter red (TAMRA fluorescence). With excitation at 488 nm, the unliganded oligonucleotide is green, reflecting only FAM fluorescence. The yellow color of the mobility-shifted band results from a combination of green and red fluorescence, indicating efficient FRET due to the wrapped DNA in the bound complex.

The lifetimes recovered from the fluorescence intensity decay data were essentially the same for all examined DNA sequences. Based on the reduction in donor lifetime (equation 1), the time-resolved FRET efficiency of 0.57 ± 0.03 yields an apparent distance of 4.8 ± 0.1 nm. This distance is comparable to the steady-state FRET distance of 5.3 nm determined by Lorenz and Diekmann (26), based on intensities determined from quantitative gel electrophoresis.

Pressure dissociation of low- and high-deformation specific IHF–DNA complexes

The ability of high-pressure perturbation to dissociate macromolecular complexes is well-documented (36–39). The effect of pressure on chemical equilibrium is expressed by

$$K_a = e^{-G^\circ/RT} = e^{-(\Delta E^\circ + p\Delta V^\circ - T\Delta S^\circ)/RT} \quad (3)$$

where K_a is the equilibrium association constant and ΔG°, ΔE°, ΔV° and ΔS° are the standard change in free energy, internal energy, volume and entropy, respectively at pressure p, temperature T and R is the gas constant. According to Le Chatelier's Principle, application of pressure drives equilibrium towards association or dissociation, depending upon which condition occupies the least volume, according to the relationship

$$\delta (\ln K_a)/\delta p = -\Delta V^\circ/RT \quad (4)$$

Figure 3 shows the effect of pressure on FRET resulting from the complex formed between IHF and

oligonucleotide A.6 at 100 nM NaCl, 10 nM oligonucleotide and 25 nM IHF. This molar ratio of DNA to IHF and the sub-nanomolar affinity of the DNA sequences for IHF assured saturation of the oligonucleotide at atmospheric pressure. The donor/acceptor emission intensity ratio of the protein-free oligonucleotide is pressure dependent in the absence of FRET and decreases continuously with increasing pressure as shown in Figure 3A (see Methods section). The addition of IHF causes about a 3-fold decrease in the emission intensity ratio at atmospheric pressure, which is indicative of FRET. With increasing pressure, these data parallel the baseline for about 300 bar followed by an increase in the emission intensity ratio as the IHF–DNA complex dissociates. The transition midpoint is near 750 bar. Convergence with the baseline, which occurs between 1250 and 1500 bar, indicates complete dissociation of the IHF–DNA complex at these pressures. In this and all other cases, the data obtained with decreasing pressure, on the return to atmospheric pressure, superimposes on the data obtained with increasing pressure. This indicates that IHF dissociation from the Series A oligonucleotides is a thermodynamically reversible process.

Baseline-corrected pressure-perturbation curves for oligonucleotides A.2 and A.6 are compared in Figure 3B. These two oligonucleotides represent sequences of low- and high-deformation energy, respectively (Table 1). The most salient feature of the two curves is that the transition midpoints of the two complexes are separated by ~500 bar, the higher-deformation energy sequence having the lower-pressure transition midpoint. The equilibrium association constant at pressure p, $K_{a,p}$, is related to the equilibrium constant at atmospheric pressure, $K_{a,atm}$, by

$$\ln K_{a,p} = \ln K_{a,atm} - p\Delta V/RT \quad (5)$$

(assuming no dependence of ΔV on p). Thus, the difference in transition midpoints could be due to a difference either in $\Delta G_{atm} = -RT \ln K_{a,atm}$, ΔV or both. However, a second notable feature of the progress curves is that the slopes of the transitions for the two sequences differ significantly. According to equation 5, a steeper slope indicates a larger negative ΔV upon dissociation.

The pressure-dependent dissociation was analyzed by assuming a binary model in which the fraction bound at pressure p is given by the appropriate root of the quadratic equation

$$f_b = (1/(2[D_o])) * \left((1/K_{a,p} + [D_o] + [P_o]) - \sqrt{(1/K_{a,p} + [D_o] + [P_o])^2 - (4[D_o][P_o])}\right) \quad (6)$$

where $[D_o]$ and $[P_o]$ are the total concentrations, respectively, of oligonucleotide and active IHF. Accounting for uncertainty in the determination of the bound and unbound state endpoints, the apparent fraction bound is related to the fraction bound by

$$f_{b,app} = f_i - (f_f - f_i)f_b \quad (7)$$

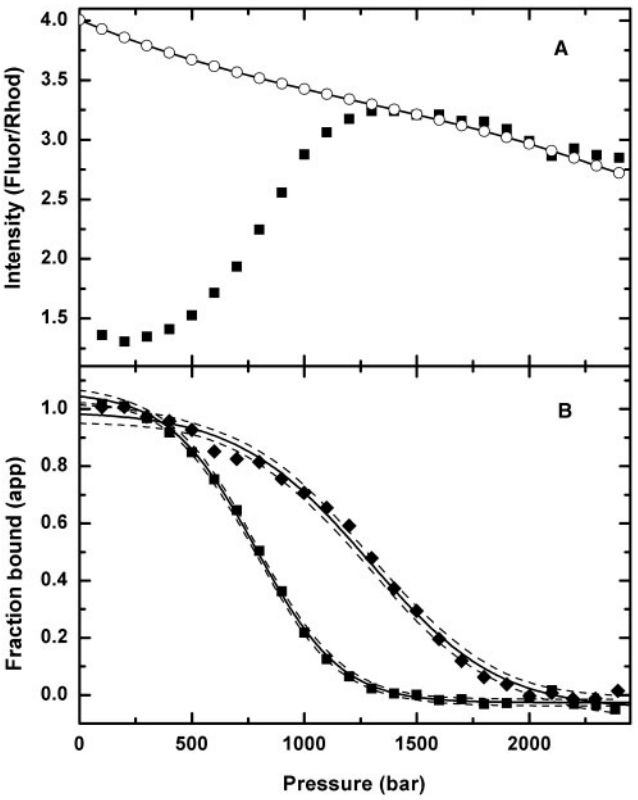

Figure 3. Panel A shows the pressure FRET ratio baseline data (open circle) and polynomial smoothing curve (solid line) for oligonucleotide A.6 in the absence of IHF compared with unprocessed data for 10 nM DNA and 25 nM IHF (filled square) (10 mM Tris pH 8.0, 100 mM NaCl and 1 mM EDTA). Panel B compares fraction bound for oligonucleotides A.2 (filled diamond) and A.6 (filled square) at 10 nM DNA, 25 nM IHF, i.e. same A.6 data as panel A and same reaction conditions. Solid and dashed curves are the fits and 95% confidence intervals to these individual experiments, using equations (5–7) as described in the text.

Pressure-perturbation curves were analyzed using equations 5, 6 and 7, with $\ln K_{a,atm}$, ΔV, f_i and f_f as adjustable parameters. This analysis from the data shown in Figure 3B yielded $\Delta G_{atm} = -13.2 \pm 0.2$ kcal mol^{-1} for formation of both complexes. This finding is consistent with the previous gel-shift results (19), which indicated that the free energy changes for dissociation of these two complexes are indistinguishable at similar low monovalent salt concentration but when divalent cations also are present (4 mM $MgCl_2$). Thus, the difference in the pressure curves for oligonucleotides A.2 and A.6, the latter being the less flexible sequence, can be attributed entirely to ΔV, for which we obtained values of 95 ± 6.5 and 151 ± 4.8 ml mol^{-1}, respectively. It should be emphasized that despite the numerical correlation between the fitting parameters $\ln K_{a,atm}$ and ΔV, both parameters were obtained with good precision from individual pressure-perturbation curves.

Consistent with the expectation from mass action that the extent of binding for a pressure-dependent

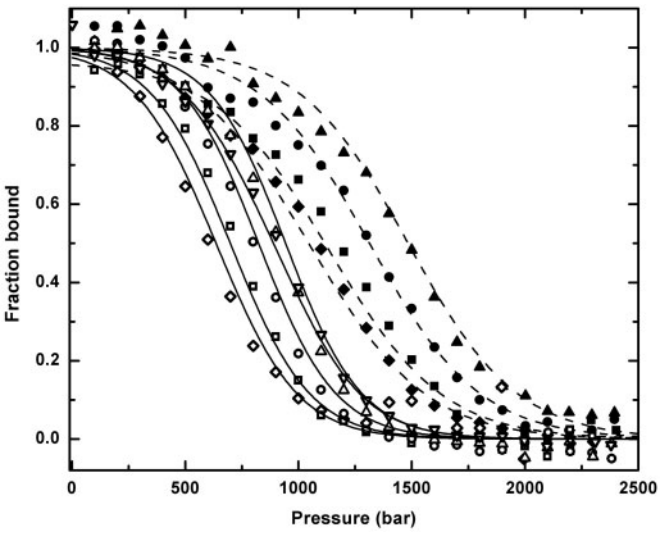

Figure 4. Global analyses of pressure-perturbation curves for oligonucleotides A.2 (solid symbols, broken lines) and A.6 (open symbols and solid lines). The component concentrations are: 3 nM DNA, 9 nM IHF (filled diamond); and 10 nM DNA at 12.5 nM IHF (filled square, open square), at 25 nM IHF (filled circle, open circle) and at 50 nM IHF (filled triangle, open triangle).

association at thermodynamic equilibrium will depend on the concentrations of the interacting components (41), the pressure-dissociation curves shift to higher or lower pressures as the concentration of DNA and/or IHF are increased or decreased, respectively (Figure 4). Because ΔV is obtained precisely from an individual pressure-perturbation curve, the concentration-dependent shift in the pressure-dissociation curves can be used to assess whether any mass action driven process other than binding of dimeric IHF to DNA contributes to ΔV. Analysis of the individual pressure-perturbation curves for each oligonucleotide obtained at different concentrations of both IHF and DNA yielded very similar estimates of $\triangle G_{atm}$ and ΔV. For example, the average values from seven determinations for oligonucleotide A.6 using concentrations ranging from 3 to 30 nM and IHF concentrations ranging from 9 to 50 nM, were $\triangle G_{atm} = -13.5 \pm 0.5$ kcal mol^{-1} and $\triangle V = 162 \pm 19$ ml mol^{-1}. There was no systematic trend in either $\triangle G_{atm}$ or ΔV as a function of either DNA or IHF concentration. Based on this observation, we conclude that only IHF–DNA binding contributes to the apparent volume change. To obtain the most accurate estimates, all of the pressure-perturbation transitions for each oligonucleotide were subsequently analyzed globally with ΔG_{atm} and ΔV as common parameters (Table 2). Examples of the global fits from oligonucleotides A.2 and A.6 at 100 mM salt at varying concentrations of DNA and IHF, but with the mole amount of IHF always in excess of DNA, are shown in Figure 4.

Experiments were also conducted at different NaCl concentrations to investigate whether thermodynamic linkage to either ion uptake or release might be coupled to DNA flexibility. These experiments were conducted at

Table 2. Volume changes for IHF binding to *de novo* synthetic sites

Site	ΔV_{spec} (ml mol^{-1})	ΔG_{spec} (kcal mol^{-1})	χ^2_{red}	No. of expts	Def. energy (kcal mol^{-1})
A.2	112 ± 8.0	-13.8 ± 0.25	1.60	4	87
A.3	131 ± 9.3	-12.3 ± 0.21	1.05	3	92
A.6	154 ± 8.0	-13.2 ± 0.15	1.64	5	142

Note: Results from pressure dissociation of binary complexes formed by sequence-specific binding of IHF to *de novo* sequences designed to vary the DNA deformation energy in the complex. Sequences contain the complete complement of consensus sequence elements as described in the text; the remaining sequence varies to generate the widest possible range of deformation energy. Values of the volume change (ΔV_{spec}) free energy change for specific binding (ΔG_{spec}) were obtained by global analysis of pressure-dissociation curves obtained with varying concentrations of IHF ranging from 9 to 50 nM and of DNA oligonucleotide ranging from 3 to 30 nM, as described in the text.

Table 3. Salt dependence of IHF binding to de novo synthetic sites

Site	ΔV_{spec}[a] (ml mol^{-1})	[NaCl] (mM)	ΔG_{spec} (kcal mol^{-1})	χ^2_{red}
A.2	112	100	-13.6 ± 0.08	1.06
		200	-12.5 ± 0.05	
		400	-9.6 ± 0.13	
A.3	131 ± 9.3	50	-13.0 ± 0.25	1.05
		100	-12.3 ± 0.21	
		200	-9.8 ± 0.09	
A.6	154 ± 8.0	50	-13.7 ± 0.22	1.00
		100	-13.2 ± 0.19	
		200	-11.4 ± 0.15	

Note: Values of the volume change (ΔV_{spec}) and free energy change for specific binding (ΔG_{spec}) were obtained by global analysis of pressure perturbation curves obtained at varying NaCl concentration using 50 nM IHF and 10 nM DNA oligonucleotide, as described in the text. [a]ΔV_{spec} was held constant *vs.* NaCl concentrations for each oligonucleotide as discussed in the text. The value was poorly resolved in the analysis of oligonucleotide A.2, and so was held fixed at the value obtained from analysis of the data at 100 mM NaCl in Table 1.

10 nM DNA and 50 nM IHF. The increased protein concentration was necessary to drive complex formation at the higher NaCl concentrations. Similar to the results of individual experiments at constant salt concentration, we found the ΔV values for a given oligonucleotide to be independent of NaCl concentration. Based on this observation, the salt-dependent data were analyzed globally with ΔV as a common parameter. The results for the three complexes at different salt concentrations are summarized in Table 3.

The global analyses supported the observations drawn from fitting the individual experimental curves. First, the average of the global ΔG_{atm} values for the complexes formed with oligonucleotides A.2, A.3 and A.6 at 100 mM NaCl was -13.1 ± 0.8 kcal mol^{-1}. The standard deviation of <1 kcal mol^{-1} indicates that the three sequences have similar affinities for IHF. Furthermore, the small variation observed does not correlate with deformation energy. Second, in contrast, the global ΔV values are markedly different, and these vary in a systematic manner from 87 to

142 ml mol^{-1}. The complex between IHF and A.6, the least DNA flexible sequence, shows the largest volume change. Third, consistent with the findings of Record and coworkers (22,40) for IHF binding to a 34-base-pair oligonucleotide containing the λ H′ site, the binding affinities of the three Series A complexes were insensitive to salt at concentrations of 100 mM NaCl and below. The binding affinities decreased progressively above 100 mM salt. There was no observable difference in salt dependence among the three complexes.

DISCUSSION

Previously, we investigated the role of DNA deformation energy in sequence-specific DNA binding by IHF (19). In that study, we compared oligonucleotide sequences containing the four consensus elements of the canonical IHF site with sequences in which the constraints of one or more of these consensus elements was relaxed. We determined that each of the recognition elements contributes to the affinity and specificity for the canonical IHF binding site that is represented by the DNA sequence in the crystal structure of the complex. When consensus constraints are relaxed, there is a direct correlation between flexibility and binding energy: the more flexible sequences exhibit higher affinity for IHF. However, when all four recognition elements 'identical' with the crystal structure are present and only base pairs that are 'not' recognition elements are varied, e.g. the Series A sequences, the binding affinities are independent of deformation energy.

This observation suggests that the Series A sequences might have unique characteristics that compensate for their variable deformation energies: first, there could be sequence-dependent, dynamic differences in global topology, which might be observed by time-resolved FRET (25); second, there could be sequence-dependent differences in the interface between IHF and the DNA, which might be observed by measuring the volume change accompanying dissociation or third, there could be both global and local structural differences, which might be observed by the combination of time-resolved FRET and volume change.

Global topology of IHF-oligonucleotide complexes

The FRET efficiency depends on closest approach of the donor and acceptor probes as well as the dynamic range of their relative orientations. These are determined by the flexibility and length of the covalent links of the probes to the 5′ phosphate. However, probe dynamics can also be constrained by interactions with the DNA. For example, TAMRA has positive charge that is attracted by negatively charged phosphates, while FAM has negative charge and is repelled. The impact of the chemical nature of these probes was demonstrated elegantly by Clegg *et al.* (42). Using steady-state fluorescence anisotropy as an observable, they found that DNA significantly restricted the motion of rhodamine, whereas the motion of fluorescein was less affected.

The decrease in the fluorescence lifetime of the FRET donor FAM upon addition of IHF was indistinguishable for each of the Series A sequences examined. This indicates that the donor–acceptor distances at the termini of these oligonucleotides in the bent, IHF-bound complexes are very similar. In addition, the narrow confidence limits obtained in the TCSPC data analyses indicate that the lifetimes are defined very precisely. This is consistent with a narrow distance distribution between the donor and acceptor probes (25). Thus, the dynamics at the termini of different oligonucleotide sequences also appear to be very similar. Accordingly, there appears to be one dominant topological state for bent DNA in the IHF complexes. The FRET efficiency for the 50-base-pair complexes calculated from the time-resolved fluorescence lifetimes is slightly greater than that determined by Diekmann and coworkers (26), who investigated nicked and intact 55-base-pair sequences using quantitative gel electrophoresis and steady-state FRET. The steady-state FRET experiments yielded distances of about 5.3 nm, whereas we calculated smaller distances of about 4.8 nm from time-resolved FRET. The 0.5-nm difference can be ascribed either to differences in the experimental approaches or to the different length of the oligonucleotides in their study. For example, the difference in length shifts the relative orientation of the 5′ phosphates, where the probes are attached, one half turn about the axis of the DNA helix. Taking this into account, our observations fully support those of Diekman and coworkers (26). Our results indicate that the global topologies of different IHF complexes that contain all four consensus elements of the canonical sequence are indistinguishable. Thus, there is no obvious impact of differences in deformation energy on either global topology or dynamics.

Binding affinities of IHF-oligonucleotide complexes and protein-DNA interface topologies

In contrast to the time-resolved FRET data, the pressure perturbation data provide a picture of the IHF-oligonucleotide complexes that indicates structurally important differences between sequences with differing deformation energies but similar binding affinities at atmospheric pressure. The observation is that, at the same concentrations of DNA, IHF and monovalent salt, the midpoints of the pressure-dissociation curves differ substantially for the three studied IHF–DNA complexes, a difference as much as 500 bar between the least and most flexible DNA sequences. The only factors that can account for this behavior are differences in DNA affinity, differences in the volume change upon dissociation from the DNA or both.

Analysis of the progress curves for a two-state binding model indicates that differences in binding affinity are not the important factors contributing to the differences in the midpoints for dissociation; the affinities of the different complexes are experimentally indistinguishable. The distinguishing difference is the volume change. Our confidence in these results is based on several observations. First, for a given salt concentration, analyses of the individual progress curves for a particular

DNA sequence at different IHF : DNA ratios yielded comparable equilibrium constants and volume changes, consistent with simple mass action for two interacting components: IHF dimer and DNA. Second, global analyses of the combined data sets of the different IHF : DNA ratios yielded statistically satisfactory reduced chi-squared values, demonstrating that the simple interpretation of a 1:1 interaction is robust. Third, the relative affinities obtained for the three IHF binding sites under these conditions match closely with those obtained previously by gel-shift analysis (19). Several-fold higher absolute affinity obtained in the pressure experiments might be the result of different reaction conditions. For example, the divalent cation included in the gel-shift buffer (19) would be expected to compete with IHF for binding to backbone phosphates, and also tends to make the DNA more rigid (30). These effects would generate a thermodynamic penalty for IHF binding. The difference in techniques may also contribute. Compared to pressure perturbation, which is an equilibrium measurement, gel mobility-shift relies on separation of bound and free species, and accompanying kinetic effects can make an association appear weaker.

An important consideration in interpretation of the pressure perturbation data is that IHF is a dimeric protein. Sufficient pressure is expected to cause dissociation of the IHF dimers to its α and β subunits, which do not bind DNA. This makes the IHF–DNA association potentially a three-component interaction. Two considerations are convincing that IHF dimers remain tightly associated at pressures of up to 2.3 kbar. First, IHF subunits fold to form stable structures and associate to form IHF dimer only when co-expressed *in vivo* (24); α and β subunits do not fold and assemble spontaneously to form dimer when mixed *in vitro* (43). Consequently, pressure-dependent dissociation of IHF dimer is expected to be thermodynamically irreversible. However, in all cases when the reversibility of IHF–DNA pressure dissociation was checked by comparing the progress curve for dissociation while increasing pressure with the progress curve for re-association while decreasing pressure, no hysteresis was observed.

Second, significant dissociation of IHF in the pressure range up to 2.3 kbar would generate an observable thermodynamic coupling between protein–protein dissociation and DNA-dimer protein dissociation (44–46). Because our analyses do not account for this effect, any significant coupling between these two processes would result in concentration dependent ΔG_{atm} and ΔV values for the protein–DNA interaction. However, no concentration dependence is observed experimentally. In addition, any volume change contribution from protein–protein dissociation would result in overestimation of the volume change attributed to IHF–DNA dissociation. If there were significant thermodynamic coupling due to protein–protein dissociation, the overestimation would impact the higher-pressure dissociation curve more than it would the lower pressure-dissociation curve. This effect would tend to reduce the difference between the pressure-dissociation curves for the various oligonucleotides, making the volume changes upon dissociation of the different complexes appear more similar then they actually are.

Based on these considerations, we are confident that the volume changes of the three complexes differ significantly and that these volume changes reflect variations in the local structural features at the protein–DNA interface. When all four canonical recognition elements are present, it is variation in local structural features that apparently provides appropriate favorable indirect interactions that compensate for the sequence-dependent differences in deformation energies. As a result of this compensation, the 'net' binding energies are essentially the same for the different complexes. What thermodynamic and structural features could account for these compensatory effects?

A model for indirect readout of the IHF canonical complex based on pressure perturbation

The volume change in a macromolecular dissociation reaction reflects the nature of the interactions between the macromolecules. As discussed in past reviews (36–39,41,47–54), important contributions include: the ability of water to fill the accessible free volume; release or uptake of counter-ions and concomitant electrostriction of water; exposure and hydration of polar and non-polar groups; and structural dynamics of the interacting macromolecules.

Historically, pressure perturbation has been used most extensively to investigate protein–protein dissociation; there are fewer studies of protein–DNA dissociation, and protein–protein and protein–DNA interactions are intrinsically different. However, some aspects are sufficiently similar to provide a basis for comparison. For example, most protein dimer associations that have been studied can be described by a simple monomer–dimer equilibrium and have volume changes in the range of 50–170 ml mol^{-1} (41), similar to the range we observe for the dissociation of the specific IHF–DNA complexes. However, coupling between protein folding and oligomerization has been observed with a number of dimeric proteins that have specific association with DNA (39,44–46), and interpretation of the volume changes is more complex due to this coupling. By comparison, although IHF is a heterodimer, we do not observe such coupling for its specific DNA complexes.

Weber and Drickamer (37) have ascribed the general dissociating effects of pressure on oligomeric proteins to covalent constraints of the protein structure that generate imperfect packing of the atoms at subunit interfaces. Imperfect packing gives rise to free volume that becomes accessible only upon dissociation. However, X-ray crystal structures show that the atom-packing densities resulting from formation of quaternary structure appear very similar to those resulting from formation of tertiary structure (55). Thus, if imperfect packing contributes to the ΔV of dissociation, it should also lead to unfolding of single-chain proteins. Consistent with this explanation, unfolding of single-chain proteins does occur, though usually at much higher pressures than observed for dissociation of oligomeric proteins. As Weber and Drickamer (37) point out, higher pressure is usually

required for unfolding because unfolding is a first-order equilibrium between conformations, whereas dissociation is a concentration-dependent process. The perturbation required for dissociation is minimized when the concentrations of interacting components are near that defined by $K_{d,atm}$, whereas the perturbation required for unfolding usually remains large. While packing volumes in protein–DNA interfaces have not been as extensively catalogued as in protein–protein interfaces, the expectation is that imperfect packing also contributes to dissociation of protein–DNA complexes.

The closely spaced, negatively charged phosphates of DNA present a very different interaction surface for protein binding than that found at protein–protein interfaces. DNA–protein interactions generally exhibit a strong salt dependence, reflecting the polyelectrolyte nature of DNA (56,57). Given potential interactions between IHF and 23 DNA phosphates along the 'arms' of the bound complex, as are evident in the crystallographic structure of the complex (Figure 1), it would be expected that the release of 0.9 Na ions per phosphate in double-strand DNA (23,58) would generate a large salt effect. However, Record and coworkers have shown that IHF has an unusually weak salt dependence for DNA binding (22,23). In addition, they found that specific binding is characterized by negative enthalpy and entropy changes. The observation that the IHF–DNA complex has a strongly favorable enthalpy of formation is also contrary to usual expectations; the substantial DNA bending and associated unstacking of base-pairs in this complex would be enthalpically unfavorable.

To account for these observations, Record and coworkers (22,23) proposed a thermodynamic-structural model for IHF binding based on information from the high-resolution crystal structure by Rice *et al.* (3); to date, there is no high-resolution structure available for free IHF. This thermodynamic-structural model proposes that disruption of intra-molecular protein salt bridges is coupled to the specific binding of IHF to DNA. Protein cationic groups are observed in the bound complex to be sufficiently close to DNA phosphates to form hydrated ion pairs (6–8 Å). The model proposes that these cationic groups form dehydrated intra-molecular salt bridges with protein carboxylate groups (~3 Å charge separation) in free IHF. This salt bridge swapping, which is proposed to involve 6 cationic groups and 18 carboxylates on IHF plus 13 DNA phosphates, would yield a net hydration upon binding. Holbrook *et al.* (22) estimate that the net favorable heat of hydration on binding compensates for the large unfavorable heat of DNA bending and accounts for the net negative entropy. Saecker and Record (23) propose that similar interactions could provide a mechanism for DNA-wrapping in other systems.

We examined the salt dependence of IHF dissociation for the three DNA sequences and obtained results that correspond with the predictions of Record and coworkers' (22,23) model. The only notable difference we observe is slightly higher affinities at low salt. This can be accounted for by the length of the oligonucleotides and the end effects on the ion distribution (59–61). However, we find that the overall salt dependence is close to that reported (22). In particular, we observe no effect of salt on ΔG_{atm} or ΔV values at 100 mM NaCl and lower concentrations. Above this concentration, the affinity decreases monotonically as a function of increasing salt concentration, as generally observed for DNA–protein interactions. Furthermore, the salt dependences for the three IHF sites are indistinguishable. Therefore, there is no contribution of salt to either the differences in volume changes or deformation energies.

Accordingly, we propose that either packing interactions, exposure of polar or ionic groups, or some combination thereof sufficient to accommodate or electrostrict about 40 ml mol^{-1}, must be the dominant factors compensating for the observed differences in deformation energy. From Weber and Drickamer's considerations (37), we expect less-efficient packing for a protein complex formed with stiffer DNA. But to account for the differences in energetics, there also must be differences in hydration. For example, Kautzmann and coworkers (62,63) determined that protonation of protein amino groups and deprotonation of carboxyl groups, which would occur on dissolution of a salt bridge, results in volume changes of about −15 to −18 and −12 ml mol^{-1}, respectively. The sum of these volume changes is close to the ~40 ml mol^{-1} difference in free volume change between the least and most flexible Series A oligonucleotides. Putting this in perspective, the difference in volume change is equivalent to that resulting from dissolution and hydration of the equivalent of one or two dehydrated salt bridges, whereas the total number proposed to be swapped in forming the complex is 18 (22,23). The swapping of the ionic interactions also suggests that another contribution to the volume change is the structural dynamics of IHF as it undergoes conformational change in its association with different DNA sequences. The salient observation, however, is that the differences in DNA deformation energy are compensated effectively by DNA-sequence dependent geometries in the specific IHF complexes and by changes in the interactions that can be made through indirect readout at the protein–DNA interface.

ACKNOWLEDGEMENTS

We thank Phoebe Rice for giving permission to use the co-ordinate file for this IHF-λ H′ DNA structure, in which the crystallographic nick in the DNA was repaired. We also thank John Gerdes for discussions on the effects of high pressures and macromolecular interaction. The research was supported in part by the following grants: MCB-9728186 from the National Science Foundation (NSF) (DFS); NIH-68903 from the National Institutes of Health (NIH) (GWH); and CA-63317 (NIH), RR-15583 (National Center for Research Resources (NCRR), a component of NIH), and MCB-0517644 (NSF) (JBAR). M.L.O. was a recipient of a Post-doctoral Fellowship and K.A.A. was a recipient of a Pre-doctoral Fellowship from the Biomedical Informatics Training (BIT) Program of the UCI Institute for Genomics and Bioinformatics, funded by a training grant from the National Library of Medicine

(NIH/NLM T15 LM-07443). The contents of this publication are solely the responsibility of the authors and do not necessarily represent the official views of NSF, NML, NCRR or NIH. Funding to pay the Open Access publication charge was provided by the National Institutes of Health and the National Science Foundation.

Conflict of interest statement. None declared.

REFERENCES

1. Bewley,C.A., Gronenborn,A.M. and Clore,G.M. (1998) Minor groove-binding architectural proteins: structure, function, and DNA recognition. *Annu. Rev. Biophys. Biomol. Struct.*, **27**, 105–131.
2. Friedman,D.I. (1988) Integration host factor: a protein for all reasons. *Cell*, **55**, 545–554.
3. Rice,P.A., Yang,S., Mizuuchi,K. and Nash,H.A. (1996) Crystal structure of an IHF-DNA complex: a protein-induced DNA U-turn. *Cell*, **87**, 1295–1306.
4. Ali,B.M., Amit,R., Braslavsky,I., Oppenheim,A.B., Gileadi,O. and Stavans,J. (2001) Compaction of single DNA molecules induced by binding of integration host factor (IHF). *Proc. Natl Acad. Sci. USA*, **98**, 10658–10663.
5. Goodman,S.D., Nicholson,S.C. and Nash,H.A. (1992) Deformation of DNA during site-specific recombination of bacteriophage lambda: replacement of IHF protein by HU protein or sequence-directed bends. *Proc. Natl Acad. Sci. USA*, **89**, 11910–11914.
6. Hwang,D.S. and Kornberg,A. (1992) Opening of the replication origin of Escherichia coli by DnaA protein with protein HU or IHF. *J. Biol. Chem.*, **267**, 23083–23086.
7. Hatfield,G.W. and Benham,C.J. (2002) DNA topology-mediated control of global gene expression in *Escherichia coli*. *Annu. Rev. Genet.*, **36**, 175–203.
8. Sheridan,S.D., Benham,C.J. and Hatfield,G.W. (1998) Activation of gene expression by a novel DNA structural transmission mechanism that requires supercoiling-induced DNA duplex destabilization in an upstreamactivating sequence. *J. Biol. Chem.*, **273**, 21298–21308.
9. Tolleri,L. (2002) Dissertation, Universita degli Studi di Pavia e Frenze, 63–71.
10. Engelhorn,M., Boccard,F., Murtin,C., Prentki,P. and Geiselmann,J. (1995) In vivo interaction of the Escherichia coli integration host factor with its specific binding sites. *Nucleic Acids Res.*, **23**, 2959–2965.
11. Goodrich,J.A., Schwartz,M.L. and McClure,W.R. (1990) Searching for and predicting the activity of sites for DNA binding proteins: compilation and analysis of the binding sites for Escherichia coli integration host factor (IHF). *Nucleic Acids Res.*, **18**, 4993–5000.
12. Ussery,D., Larsen,T.S., Wilkes,K.T., Friis,C., Worning,P., Krogh,A. and Brunak,S. (2001) Genome organisation and chromatin structure in Escherichia coli. *Biochimie*, **83**, 201–212.
13. Rice,P.A. (1997) Making DNA do a U-turn: IHF and related proteins. *Curr. Opin. Struct. Biol.*, **7**, 86–93.
14. Hales,L.M., Gumport,R.I. and Gardner,J.F. (1994) Determining the DNA sequence elements required for binding integration host factor to two different target sites. *J. Bacteriol.*, **176**, 2999–3006.
15. Hales,L.M., Gumport,R.I. and Gardner,J.F. (1996) Examining the contribution of a dA+dT element to the conformation of Escherichia coli integration host factor-DNA complexes. *Nucleic Acids Res.*, **24**, 1780–1786.
16. Mengeritsky,G., Goldenberg,D., Mendelson,I., Giladi,H. and Oppenheim,A.B. (1993) Genetic and biochemical analysis of the integration host factor of Escherichia coli. *J. Mol. Biol.*, **231**, 646–657.
17. Wang,S., Cosstick,R., Gardner,J.F. and Gumport,R.I. (1995) The specific binding of Escherichia coli integration host factor involves both major and minor grooves of DNA. *Biochemistry*, **34**, 13082–13090.
18. Yang,C.C. and Nash,H.A. (1989) The interaction of E. coli IHF protein with its specific binding sites. *Cell*, **57**, 869–880.
19. Aeling,K.A., Opel,M.L., Steffen,N.R., Tretyachenko-Ladokhina,V., Hatfield,G.W., Lathrop,R.H. and Senear,D.F. (Oct 11, 2006) Indirect Recognition in Sequence-Specific DNA Binding by *E. coli* Integration Host Factor: the Role of DNA Deformation Energy. *J. Biol. Chem.*; doi:10.1074/jbc.M606363200.
20. Lynch,T.W., Read,E.K., Mattis,A.N., Gardner,J.F. and Rice,P.A. (2003) Integration host factor: putting a twist on protein-DNA recognition. *J. Mol. Biol.*, **330**, 493–502.
21. Travers,A. (1997) DNA-protein interactions: IHF–the master bender. *Curr. Biol.*, **7**, R252–R254.
22. Holbrook,J.A., Tsodikov,O.V., Saecker,R.M. and Record,M.T. Jr (2001) Specific and non-specific interactions of integration host factor with DNA: thermodynamic evidence for disruption of multiple IHF surface salt-bridges coupled to DNA binding. *J. Mol. Biol.*, **310**, 379–401.
23. Saecker,R.M. and Record,M.T. Jr (2002) Protein surface salt bridges and paths for DNA wrapping. *Curr. Opin. Struct. Biol.*, **12**, 311–319.
24. Nash,H.A., Robertson,C.A., Flamm,E., Weisberg,R.A. and Miller,H.I. (1987) Overproduction of Escherichia coli integration host factor, a protein with nonidentical subunits. *J. Bacteriol.*, **169**, 4124–4127.
25. Lakowicz,J.R. (1999) *Principles of Fluorescence Spectroscopy*, 2nd edn. Plenum, New York, pp 301, 368–371.
26. Lorenz,M. and Diekmann,S. (2001) Quantitative distance information on protein-DNA complexes determined in polyacrylamide gels by fluorescence resonance energy transfer. *Electrophoresis*, **22**, 990–998.
27. Lorenz,M., Hillisch,A. and Diekmann,S. (2002) Fluorescence resonance energy transfer studies of U-shaped DNA molecules. *J. Biotechnol.*, **82**, 197–209.
28. Lorenz,M., Hillisch,A., Goodman,S.D. and Diekmann,S. (1999) Global structure similarities of intact and nicked DNA complexed with IHF measured in solution by fluorescence resonance energy transfer. *Nucleic Acids Res.*, **27**, 4619–4625.
29. Wu,P. and Brand,L. (1994) Resonance energy transfer: methods and applications. *Anal. Biochem.*, **218**, 1–13.
30. Rachofsky,E.L., Osman,R. and Ross,J.B. (2001) Probing structure and dynamics of DNA with 2-aminopurine: effects of local environment on fluorescence. *Biochemistry*, **40**, 946–956.
31. Grinvald,A. and Steinberg,I.Z. (1974) On the analysis of fluorescence decay kinetics by the method of least-squares. *Anal. Biochem.*, **59**, 583–598.
32. Bevington,P.R. (1969) *Data Reduction and Error Analysis for the Physical Sciences*, 195–198.
33. Paladini,A.A. Jr and Weber,G. (1981) Absolute measurements of fluorescence polarization at high pressures. *Rev. Sci. Instrum.*, **52**, 419–427.
34. Rietveld,A.W. and Ferreira,S.T. (1996) Deterministic pressure dissociation and unfolding of triose phosphate isomerase: persistent heterogeneity of a protein dimer. *Biochemistry*, **35**, 7743–7751.
35. Box,G.D.P. (1960) Fitting empirical data. *Ann. NY Acad. Sci.*, **86**, 792–816.
36. Heremans,K. (1982) Pressure effects on proteins and other biomolecules. *Ann. Rev. Biophys. Bioeng.*, **11**, 1–21.
37. Weber,G. and Drickamer,H.G. (1983) The effect of high pressure upon proteins and other biomolecules. *Q. Rev. Biophys.*, **16**, 89–112.
38. Heremans,K. and Smeller,L. (1998) Protein structure and dynamics at high pressure. *Biochim. Biophys. Acta*, **1386**, 353–370.
39. Silva,J.L., Foguel,D. and Royer,C.A. (2001) Pressure provides new insights into protein folding, dynamics and structure. *Trends Biochem. Sci.*, **26**, 612–618.
40. Tsodikov,O.V., Holbrook,J.A., Shkel,I.A. and Record,M.T. Jr (2001) Analytic binding isotherms describing competitive interactions of a protein ligand with specific and nonspecific sites on the same DNA oligomer. *Biophys. J.*, **81**, 1960–1969.
41. Silva,J.L. and Weber,G. (1993) Pressure stability of proteins. *Annu. Rev. Phys. Chem.*, **44**, 89–113.
42. Clegg,R.M., Murchie,A.I., Zechel,A. and Lilley,D.M. (1993) Observing the helical geometry of double-stranded DNA in solution by fluorescence resonance energy transfer. *Proc. Natl Acad. Sci. USA*, **90**, 2994–2998.
43. Wang,H. and Chong,S. (2003) Visualization of coupled protein folding and binding in bacteria and purification of the heteromeric complex. *Proc. Natl Acad. Sci. USA*, **100**, 478–3.

44. Silva,J.L. and Silveira,C.F. (1993) Energy coupling between DNA binding and subunit association is responsible for the specificity of DNA-Arc interaction. *Protein Sci.*, **2**, 945–950.
45. Silva,J.L., Silveira,C.F., Correia Junior,A. and Pontes,L. (1992) Dissociation of a native dimer to a molten globule monomer. Effects of pressure and dilution on the association equilibrium of arc repressor. *J. Mol. Biol.*, **223**, 545–555.
46. Peng,X., Jonas,J. and Silva,J.L. (1994) High-pressure NMR study of the dissociation of Arc repressor. *Biochemistry*, **33**, 8323–8329.
47. Cioni,P. and Strambini,G.B. (1996) Pressure effects on the structure of oligomeric proteins prior to subunit dissociation. *J. Mol Biol.*, **263**, 789–799.
48. Meersman,F., Smeller,L. and Heremans,K. (2006) Protein stability and dynamics in the pressure-temperature plane. *Biochim. Biophys. Acta*, **1764**, 346–354.
49. Mozhaev,V.V., Heremans,K., Frank,J., Masson,P. and Balny,C. (1996) High pressure effects on protein structure and function. *Proteins*, **24**, 81–91.
50. Weber,G., Tanaka,F., Okamoto,B.Y. and Drickamer,H.G. (1974) The effect of pressure on the molecular complex of isoalloxazine and adenine. *Proc. Natl Acad. Sci. USA*, **71**, 1264–1266.
51. Chalikian,T.V. (2003) Volumetric properties of proteins. *Annu. Rev. Biophys. Biomol. Struct.*, **32**, 207–235.
52. Chalikian,T.V. and Breslauer,K.J. (1998) Volumetric properties of nucleic acids. *Biopolymers*, **48**, 264–280.
53. Chalikian,T.V. and Breslauer,K.J. (1998) Thermodynamic analysis of biomolecules: a volumetric approach. *Curr. Opin. Struct. Biol.*, **8**, 657–664.
54. Barciszewski,J., Jurczak,J., Porowski,S., Specht,T. and Erdmann,V.A. (1999) The role of water structure in conformational changes of nucleic acids in ambient and high-pressure conditions. *Eur. J. Biochem.*, **260**, 293–307.
55. Richards,F.M. (1977) Areas, volumes, packing and protein structure. *Annu. Rev. Biophys. Bioeng.*, **6**, 151–176.
56. Manning,G.S. (1978) The molecular theory of polyelectrolyte solutions with applications to the electrostatic properties of polynucleotides. *Q. Rev. Biophys.*, **11**, 179–246.
57. Record,M.T. Jr, Anderson,C.F. and Lohman,T.M. (1978) Thermodynamic analysis of ion effects on the binding and conformational equilibriums of proteins and nucleic acids: the roles of ion association or release, screening, and ion effects on water activity. *Q. Rev. Biophys.*, **11**, 103–178.
58. Record,M.T. Jr, Zhang,W. and Anderson,C.F. (1998) Analysis of effects of salts and uncharged solutes on protein and nucleic acid equilibria and processes: a practical guide to recognizing and interpreting polyelectrolyte effects, Hofmeister effects, and osmotic effects of salts. *Adv. Protein Chem.*, **51**, 281–353.
59. Olmsted,M.C., Anderson,C.F. and Record,M.T. Jr (1989) Monte Carlo description of oligoelectrolyte properties of DNA oligomers: range of the end effect and the approach of molecular and thermodynamic properties to the polyelectrolyte limits. *Proc. Natl Acad. Sci. USA*, **86**, 7766–7770.
60. Stein,V.M., Bond,J.P., Capp,M.W., Anderson,C.F. and Record,M.T. Jr (1995) Importance of coulombic end effects on cation accumulation near oligoelectrolyte B-DNA: a demonstration using 23Na NMR. *Biophys. J.*, **68**, 1063–1072.
61. Zhang,W., Ni,H., Capp,M.W., Anderson,C.F., Lohman,T.M. and Record,M.T. Jr (1999) The importance of coulombic end effects: experimental characterization of the effects of oligonucleotide flanking charges on the strength and salt dependence of oligocation (L8+) binding to single-stranded DNA oligomers. *Biophys. J.*, **76**, 1008–1017.
62. Kauzmann,W., Bodanszky,A. and Rasper,J. (1962) Volume changes in protein reactions. II. Comparison of ionization reactions in proteins and small molecules. *J. Am. Chem. Soc.*, **84**, 1777–1788.
63. Rasper,J. and Kauzmann,W. (1962) Volume changes in protein reactions. I. Ionization reactions of proteins. *J. Am. Chem. Soc.*, **84**, 1771–1777.